Originalarbeit

Elektrotech. Inftech. (2023) 140:338–351
https://doi.org/10.1007/s00502-023-01128-2

e+i elektrotechnik und informationstechnik

Efficient modeling of DFIG- and FSC-based wind turbines for frequency stability analysis

Farshid Goudarzi · Lucas Reus · Lutz Hofmann

Received: 27 October 2022 / Accepted: 8 February 2023 / Published online: 13 March 2023

Abstract The contribution of wind turbines (WTs) to enhance the frequency stability of power systems is traditionally analyzed using commonly applied root mean square (RMS) models. RMS WT models require smaller simulation time steps compared to conventional active devices (i.e., synchronous generators and dynamic loads) due to the comparatively smaller time constants of the converter controllers. Such small time steps become relevant in simulations of large-scale power systems with a high level of WT penetration and lead to high computational time and effort. This paper presents simplified simulation models of a doubly-fed induction generator-based WT and a full-scale converter-based WT, which enable higher simulation time steps due to the negligence of very small time constants with no relevant effects in the time frame of interest of frequency stability analysis. The models are derived from detailed RMS WT models based on fundamental machine and converter equations. In order to verify the validity of the underlying simplifications, the simplified models are compared to the detailed RMS models with a focus on their general behavior in case of step responses and their frequency responses in the event of a frequency drop in a 220 kV test system. For this purpose, both the detailed RMS WT models as well as the simplified WT models are extended with a droop-based fast frequency response controller and implemented in a MATLAB-based RMS simulation tool. The results of the case studies show feasible and comparable general behavior of the WT models as well as plausible frequency responses.

F. Goudarzi (✉) · L. Reus · L. Hofmann
Leibniz University Hannover, Institute of Electric Power Systems, Appelstraße 9a, 30167 Hanover, Germany
goudarzi@ifes.uni-hannover.de

Keywords Doubly-fed induction generator · Efficient modeling · Frequency stability analysis · Full-scale converter · Model reduction · Wind turbine modeling

Effiziente Modellierung von Windenergieanlagen mit doppelt gespeister Asynchronmaschine und Vollumrichter für Untersuchungen der Frequenzstabilität

Zusammenfassung Der Beitrag von Windenergieanlagen (WEA) zur Erhöhung der Frequenzstabilität wird klassischerweise mit quasistationären Modellen untersucht. Die Verwendung quasistationärer Modelle von WEA erfordert, aufgrund der im Vergleich zu konventionellen aktiven Betriebsmitteln (wie Synchronmaschinen oder dynamischen Lasten) kleineren Zeitkonstanten der Umrichterregelung, kleinere Zeitschritte in der Simulation. Diese kleinen Zeitkonstanten werden relevant bei der Simulation ausgedehnter Elektroenergiesysteme mit hohem Anteil von WEA und führen zu hohen Rechenzeiten. In dieser Veröffentlichung werden vereinfachte Modelle für WEA mit doppelt gespeister Asynchronmaschine bzw. mit Vollumrichter vorgestellt. Durch die Vernachlässigung kleiner Zeitkonstanten ohne größere Auswirkungen im Zeitbereich der Frequenzstabilität können die Zeitschritte der Simulation deutlich erhöht werden. Die Modelle werden aus detaillierten quasistationären Modellen abgeleitet, die auf den grundlegenden Gleichungen der Maschinen und Umrichter basieren. Um die Gültigkeit der getroffenen Vereinfachungen zu bestätigen, werden die vereinfachten mit den detaillierten quasistationären Modellen verglichen. Der Fokus liegt dabei auf der Sprung- und Frequenzantwort im Falle eines Frequenzeinbruchs in einem 220-kV-Testsystem. Für die Untersuchungen werden die vereinfachten und die detaillierten Modelle um einen auf einer Statik basierenden Fast Frequency Response-

Regler ergänzt und in einem quasistationären Simulationstool in MATLAB implementiert. Die Ergebnisse der Fallstudien zeigen plausible und vergleichbare Verhalten der Modelle der WEA sowie plausible Frequenzverläufe.

Schlüsselwörter Doppelt gespeister Asynchrongenerator · Effiziente Modellierung · Frequenzstabilitätsuntersuchungen · Vollumrichter · Reduzierte Modelle · Modellierung von Windenergieanlagen

1 Introduction

The ongoing displacement of conventional power plants by power electronic-interfaced generating units (PEGU) leads to a gap caused by the missing contribution of synchronous generators to overcome the stability issues following a perturbation, which needs to be filled by the PEGU. In order to analyze the contributions of PEGU to the power system stability, the first essential step is to utilize appropriate dynamic simulation models for investigating the respective stability phenomenon. The applied simulation models shall be valid regarding the following three requirements: the time frame of interest (i.e., short- or long-term), modeling depth (i.e., electromagnetic transient [EMT] or root mean square [RMS]) and the width of the grid area to be studied.

Frequency stability studies are traditionally conducted using RMS simulations, which are capable of simulating much longer events and much larger grid areas compared to EMT simulations [14, 18–20]. The RMS wind turbine (WT) models used in frequency stability studies, which are designed based on fundamental machine and converter equations and are also known as quasi-stationary models in the literature, require smaller simulation time steps compared to the conventional active devices (i.e., synchronous generators and dynamic loads) due to comparatively smaller time constants of the converter controllers [6, 10]. However, in large-scale studies considering a high share of WTs, the small simulation time steps become more relevant and lead to long computational time and high effort.

This paper presents simplified simulation models of a doubly fed induction-generator-based (DFIG-based) WT and a full-scale-converter-based (FSC-based) WT neglecting the small time constants mentioned above without loss of accuracy of results. The models are each developed on the basis of a detailed RMS WT model, which is extensively discussed in [8]. The simplifications include assuming the control loops of both the machine-side converter (MSC) and grid-side converter (GSC) as well as the rotor flux linkage components, as the electrical state variables of the RMS induction generator model, to be quasi-stationary. Furthermore, the commonly used two-mass model of the drive train is reduced to a lumped model. The negligence of state variables corresponding to very small time constants is without significant effects on the behavior of the WT within the time frame of interest and enables higher simulation time steps and thus significantly lower simulation time. The considerably smaller number of state variables of the simplified WT models compared to the detailed RMS WT models results in less model complexity and thus less parametrization effort. In order to verify the validity of the simplifications mentioned above, the frequency behavior of the simplified WT models are compared against those of the detailed models. For this purpose, all detailed as well as simplified models are programmed in the MATLAB environment and are implemented in a MATLAB-based RMS simulation tool, which is discussed in [16, 17]. Furthermore, they are extended with a droop-based fast frequency response (FFR) controller. The results of the case studies demonstrate an acceptable level of model accuracy in the time frame of frequency stability studies. The models discussed in this paper are suitable for the investigation of balanced events in the network, and therefore only their positive sequence representations are taken into consideration. Furthermore, the equations are given on the principle of SI base units and the passive sign convention is chosen, so that consumed active and reactive powers are positive quantities.

Following the introduction, Sect. 2 treats briefly the modeling approach of the detailed RMS DFIG-based WT model and the FSC-based WT model using an induction generator. Afterwards, the underlying simplifications and the resulting simplified WT models are explained in Sect. 3. While Sect. 4 deals with the implemented droop-based FFR controller, the advantages of the simplified WT models are explained in Sect. 5. Case studies and their results demonstrating some characteristic variables of step response simulations of detailed and simplified WT models to different deterministic wind speeds as well as their performance in case of a frequency drop in a 220 kV test system are compared and discussed in Sect. 6.

2 Detailed models of Wind turbines

The detailed simulation models of the DFIG-based WT and the FSC-based WT using induction generators are comprehensively explained in [8], which is why they are treated very roughly in this paper. Both of them comprise sub-modules to represent the aerodynamics of the rotor blades, the drive train and the induction generator as well as the controllers for the pitch angle, the rotor speed and the GSC and MSC, which are discussed in the following.

2.1 DFIG-based WT model

The overall control system of a variable-speed WT based on a DFIG is depicted in Fig. 1. As shown,

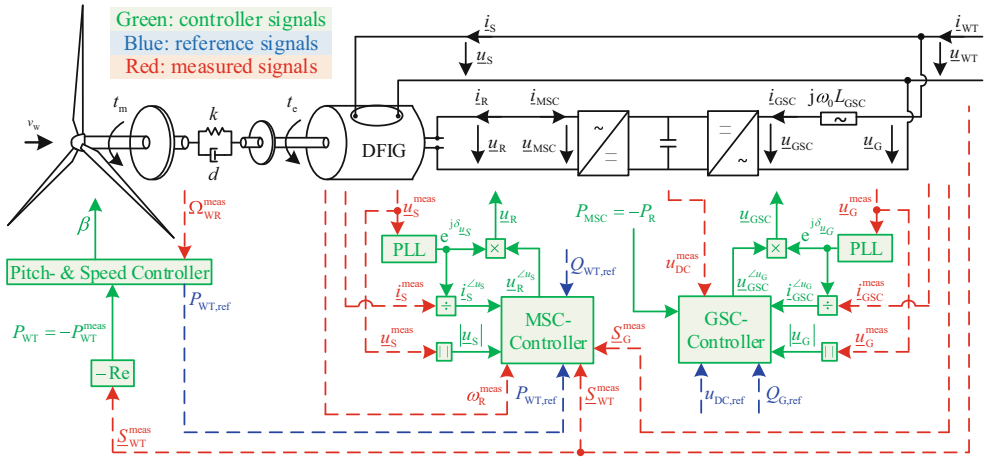

Fig. 1 The overall control system of the DFIG-based WT model [8]

the rotor terminals are coupled to the grid through a back-to-back frequency converter comprising two separately controlled voltage source converters (MSC and GSC), which are rated for a fraction of the total generator power (slip power $s_G P_{ag}$), where s_G is the slip and P_{ag} is the air-gap power. The power flow fed into the grid via the rotor circuit depends on the generator speed, whose ratio to the stator angular frequency divides the operating points of the WT into sub-synchronous, synchronous and super-synchronous operating points.

2.1.1 Aerodynamic and drive train model

The mechanical power P_m of a WT with the rotor radius $R_{W,R}$ extracted from the wind with the velocity v_W is calculated based on the aerodynamic power coefficient $c_p(\beta,\lambda)$ as a function of the pitch angle β and the tip-speed ratio λ, where ρ is the density of air [9]:

$$P_m = \frac{1}{2}\rho\pi R_{WR}^2 v_W^3 c_p(\beta,\lambda) \tag{1}$$

The drive train model is represented through a two-mass mechanical model, which is described by the following set of differential equations, where Ω_W is the wind turbine rotor speed and Ω_G is the generator rotor speed. The two masses are characterized by the larger turbine inertia time constant H_W and the smaller generator inertia time constant H_G. The coupling of both masses is considered through the stiffness k and the damping coefficient d. The gear system is represented only by a transformation ratio r_{GB} due to its negligible inertia.

$$\begin{bmatrix}\dot{\Omega}_W\\ \dot{\Omega}_G\\ \Delta\dot{\theta}\end{bmatrix} = \begin{bmatrix}\frac{-d}{2H_W} & \frac{d}{2H_W} & \frac{-k}{2H_W}\\ \frac{d}{2H_G} & \frac{-d}{2H_G} & \frac{k}{2H_G}\\ 1 & -1 & 0\end{bmatrix}\begin{bmatrix}\Omega_W\\ \Omega_G\\ \Delta\theta\end{bmatrix} + \begin{bmatrix}\frac{t_m}{2H_W}\\ \frac{t_e}{2H_G}\\ 0\end{bmatrix} \tag{2}$$

The electrical torque t_e is gained from the induction generator equations described in the next section. The mechanical torque t_m is calculated as the mechanical power divided by the WT rotor speed Ω_W referred to the fast side of the gearbox as follows:

$$t_m = \frac{P_m}{\Omega_W} \tag{3}$$

The rotor angular frequency can be calculated as follows considering the number of pole pairs p:

$$\omega_R = \frac{\Omega_G}{p} \tag{4}$$

2.1.2 Induction generator

Besides the equation of motion already included in (2), the full order model of an induction generator is formulated with the following equations using space phasors with the stator and rotor flux linkages $\underline{\psi}_S$ and $\underline{\psi}_R$, the stator and rotor voltages $\underline{u}_S$ and $\underline{u}_R$, the stator and rotor resistances R_S and R_R, the stator and rotor inductance L_S and L_R as well as the magnetizing inductance L_m [13]:

$$\underline{u}_S = R_S\underline{i}_S + j\omega_S\underline{\psi}_S + \dot{\underline{\psi}}_S \tag{5}$$

$$\underline{u}_R = R_R\underline{i}_R + js_G\omega_S\underline{\psi}_R + \dot{\underline{\psi}}_R \tag{6}$$

$$\underline{\psi}_S = L_S\underline{i}_S + L_m\underline{i}_R \tag{7}$$

$$\underline{\psi}_R = L_R\underline{i}_R + L_m\underline{i}_S \tag{8}$$

The equations are expressed in a rotating reference frame containing orthogonal direct (d) and quadrature (q) axes at the arbitrary stator angular frequency ω_S, where the slip is defined as $s_G = (\omega_S - \omega_R)/\omega_S$. In a RMS representation of the induction generator, the fast stator transients are assumed to be already decayed by neglecting the derivative term of the stator flux linkage in (5), i.e., $\dot{\underline{\psi}}_S = 0$. The electrical differential equation system of the generator is formulated through eliminating $\underline{i}_R$ in (6) using (8), where $k_R = L_m/L_R$:

$$\begin{bmatrix}\dot{\psi}_{Rd}\\ \dot{\psi}_{Rq}\end{bmatrix} = \begin{bmatrix}-\frac{R_R}{L_R} & s_G\omega_S\\ -s_G\omega_S & -\frac{R_R}{L_R}\end{bmatrix}\begin{bmatrix}\psi_{Rd}\\ \psi_{Rq}\end{bmatrix} + k_R R_R\begin{bmatrix}i_{Sd}\\ i_{Sq}\end{bmatrix} + \begin{bmatrix}u_{Rd}\\ u_{Rq}\end{bmatrix} \tag{9}$$

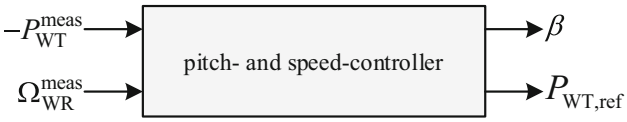

Fig. 2 The summarized block diagram of the pitch- and speed-controller

The electrical torque t_{e} can be calculated as follows:

$$t_{\mathrm{e}} = -\frac{3}{2} p k_{\mathrm{R}} \mathrm{Im}\left\{\underline{\psi}_{\mathrm{R}} \underline{i}_{\mathrm{S}}^{*}\right\} \tag{10}$$

Since the stator terminals of the DFIG are directly coupled to the grid, ω_{S} is replaced by the grid synchronous angular frequency ω_0.

2.1.3 Pitch and speed controller

Since the pitch and the speed controller including the active power–rotor speed tracking characteristic of the simplified model are exactly adopted from the detailed RMS model, they are not explained in detail below. They are summarized as a block diagram with the input variables being the measured values of the WT active power $-P_{\mathrm{WT}}^{\mathrm{meas}}$ and the WT rotor speed $\Omega_{\mathrm{WR}}^{\mathrm{meas}}$ and the output variables being the pitch angle β and the WT reference active power $P_{\mathrm{WT,ref}}$, as depicted in Fig. 2. As mentioned above, a detailed description of these sub-modules can be found in [8].

2.1.4 Machine-side converter controller

The function of the MSC controller is the independent control of the active and reactive power at the WT terminals. The MSC controller is divided into a faster inner rotor current control loop and a slower outer power control loop. The inner control loop calculates the impressed rotor voltage whereas the outer control loop determines the rotor current reference value. The applied control strategy is designed utilizing a vector control approach in a stator-voltage-oriented dq-reference frame, which is indicated through the superscript $\angle u_{\mathrm{S}}$ and feeding the rotor terminals with a voltage of variable frequency and amplitude. The controller structure is based on the stationary form of the DFIG equation system and is illustrated in Fig. 3. A comprehensive derivation of the control concept is discussed in [8]. In order to avoid redundant information, a detailed description is not provided in this paper.

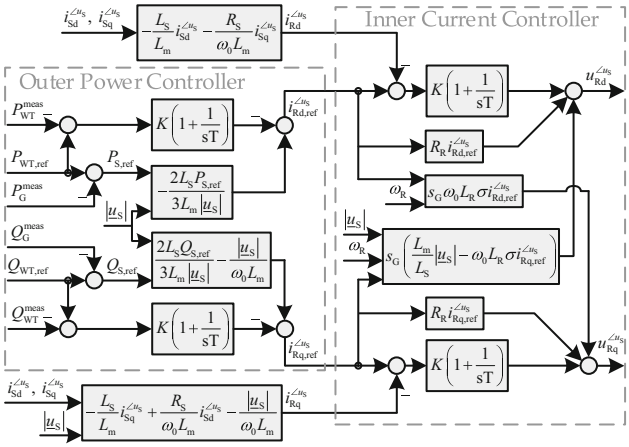

Fig. 3 Block diagram of the MSC controller of the DFIG-based WT model [7]

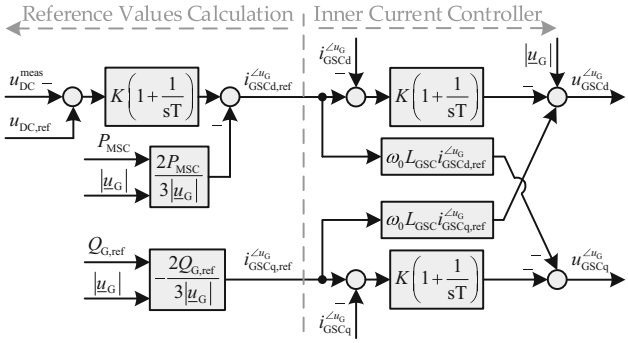

Fig. 4 Block diagram of the GSC controller of the DFIG-based WT model [8]

2.1.5 Grid-side converter controller

The function of the GSC controller is to ensure the transition of the active power from the DC-link to the grid while maintaining the DC voltage as well as to contribute to grid voltage support during steady-state and dynamic operation via reactive power provision. The GSC controller consists of an inner current control loop and an outer control loop to calculate the current reference value. The control approach is conceptualized in a dq-reference frame, which rotates with ω_0 and is oriented to the terminal voltage of the GSC. The orientation of the reference frame is denoted by the superscript $\angle u_{\mathrm{G}}$. The derivation of the applied control concept is extensively explained in [8] and is represented here only through its block diagram (see Fig. 4).

2.2 FSC-based WT model

The overall control system of the variable-speed FSC-based WT is illustrated in Fig. 5. As shown, the stator terminals are coupled to the grid through a back-to-back frequency converter comprising two independently controlled voltage source converters (MSC and GSC). As a result, the entire power of the generator is fed into the grid via the frequency converter, which results in a higher rated power compared to converters of DFIG-based WTs. The aerodynamic and drive train model, the induction generator, the pitch and speed controller as well as the GSC controller remain unchanged and are implemented in the same way as explained in the previous sections for the DFIG-based WT model. The only difference is setting $\underline{u}_{\mathrm{R}}$ in the induction generator equations to zero (squirrel-cage induction generator SCIG), which is why the sli

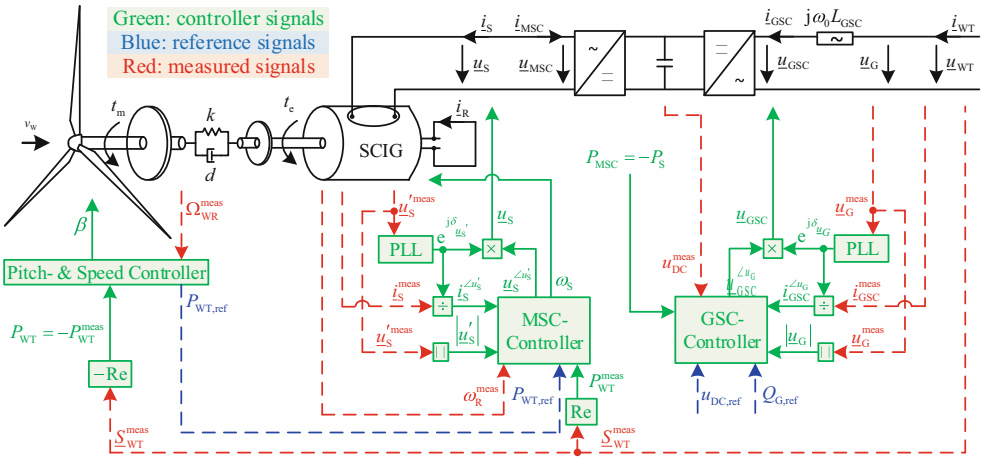

Fig. 5 The overall control system of the FSC-based WT model [8]

p power $s_G P_{ag}$ is wasted as rotor losses in the rotor circuit ($P_R = P_{RV} = 3/2\ R_R|\underline{i}_R|^2$). The MSC controller is the only model-specific sub-module that is treated in the following section.

2.2.1 Machine-side converter controller

The function of the MSC controller is to control the active power output of the WT according to the optimization of the power extracted from the incoming wind, which is realized through a stator current control. The controller is divided into an inner stator current control loop and an outer power control loop. The inner control loop calculates the impressed stator voltage $\underline{u}_S$ whereas the outer control loop determines the d-component of the stator current reference value $i_{Sd,ref}^{\angle u'_S}$. The applied control strategy is designed utilizing a vector control approach in a transient-voltage-oriented dq-reference frame, which is indicated through the superscript $\angle u'_S$ and feeding the stator terminals with a voltage of variable frequency and amplitude. The controller structure is based on the stationary form of the SCIG equation system and is illustrated in Fig. 6. A comprehensive derivation of the control concept is discussed in [8].

2.3 Norton equivalent circuits

In RMS simulation, the WT models are represented in the overall network nodal equation system by their Norton equivalent circuits, whose current sources depend on the state variables of the differential equations. The overall equivalent circuit of the DFIG-based WT consists of the Norton equivalent circuits of the DFIG and the GSC, as shown in Fig. 7a, where $\underline{u}'_S = j\omega_S k_R \psi_R$, $\underline{Z}'_S = R_S + j\omega_S L'_S$ and $\underline{Z}_{GSC} = j\omega_0 L_{GSC}$. Since all sub-modules of the FSC-based WT except the GSC are fully decoupled from the grid via the DC-link of the frequency converter, the equivalent circuit of the FSC-based WT is represented by the Norton equivalent circuit of the GSC, as shown in Fig. 7b.

3 Simplified models of wind turbines

The simplified WT models are developed based on the detailed RMS DFIG-based and FSC-based WT models discussed above. The sub-modules of the aerodynamic model as well as the pitch and the speed controller, including the active power–rotor speed tracking characteristic, are exactly adopted from the detailed RMS models, which are roughly treated in

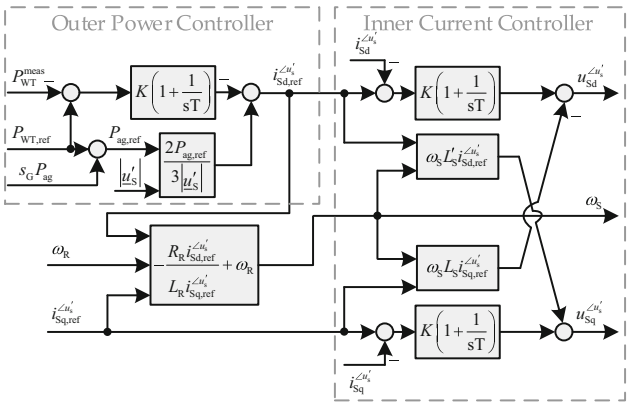

Fig. 6 Block diagram of the MSC controller of the FSC-based WT model [8]

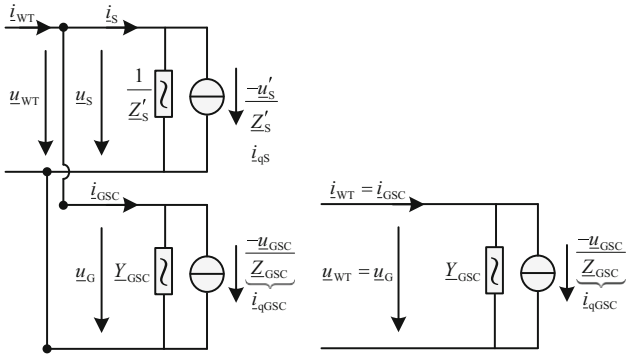

Fig. 7 Norton equivalent circuits of **a** the DFIG-based WT model and **b** the FSC-based WT model [8]

Sect. 2 and explained in a detailed manner in [8]. The underlying model simplifications are discussed below. The two-mass model of the drive train is replaced by a lumped model with a single mass, which is described by the following equation, where Ω_R is the rotor speed. The total inertia time constant H_{WT} represents the aggregated mass of the rotor blades, rotor hub as well as the turbine and generator shafts.

$$\dot{\Omega}_R = \frac{1}{2H_{WT}}(t_m + t_e) \tag{11}$$

The rotor flux linkage components of the RMS model of the induction generator as the electrical state variables are assumed to be quasi-stationary, i.e., $\dot{\underline{\psi}}_{Rd} = 0$ and $\dot{\underline{\psi}}_{Rq} = 0$. Thus, the dynamic behavior of the induction generator is represented through its only differential equation, i.e., the equation of motion (11). In order to neglect the small time constants of the MSC and the GSC controllers without considerable impact on the behavior of the WT within the time frame of interest, their control loops are assumed to be quasi-stationary. Against this background, the induction generator and the MSC are represented together based on the steady-state model of the induction generator in its original reference frame. Since no orientation of the reference frame to the stator voltage and the terminal voltage is performed in the case of the DFIG-based WT model and no orientation of the reference frame to the transient voltage and the terminal voltage is executed in the case of the FSC-based WT model, no orientation angles and thus no utilization of a Phase-Locked-Loop (PLL) is required.

3.1 DFIG-based WT model

Since the PI controllers of the MSC controller in Fig. 3 are assumed to be quasi-stationary, the rotor current reference value $\underline{i}_{R,ref}$ can be calculated using the feed forward terms of the outer power controller loop retransformed from the stator-voltage-oriented reference frame into the original reference frame of the induction generator in complex notation as follows:

$$\underline{i}_{R,ref} = -\frac{2L_S}{3L_m}\left(\frac{P_{S,ref} + jQ_{S,ref}}{\underline{u}_S}\right)^* - j\frac{\underline{u}_S}{\omega_0 l_m} \tag{12}$$

Taking into account the quasi-stationary assumption of the inner current controller, the rotor current is set to the rotor current reference value, i.e., $\underline{i}_R = \underline{i}_{R,ref}$. Furthermore, the rotor voltage can be derived from the feed forward terms of the inner current controller loop retransformed from the stator-voltage-oriented reference frame into the original reference frame of the induction generator in complex notation:

$$\underline{u}_R = \left(R_R + j s_G \omega_0 L_R \sigma\right)\underline{i}_R + s_G \frac{L_m}{L_S}\underline{u}_S \tag{13}$$

The rotor flux linkage, which is needed to calculate the electrical torque using (10), can be obtained from (8). Considering the stator current as a function of the apparent stator power reference, the current source of the Norton equivalent circuit of the DFIG can be calculated as follows:

$$\underline{i}_{qS} = \underline{i}_S - \frac{\underline{u}_S}{\underline{Z}'_S} = \frac{2}{3}\left(\frac{P_{S,ref} + jQ_{S,ref}}{\underline{u}_S}\right)^* - \frac{\underline{u}_S}{\underline{Z}'_S} \tag{14}$$

Since the DC voltage and thus the DC voltage controller are assumed to be also quasi-stationary, i.e., $\dot{u}_{DC} = 0$ and $u_{DC}^{meas} = u_{DC,ref}$, and thus the transients of the DC voltage are assumed to be decayed in the time frame of interest, a power equilibrium at the DC node can be permanently assumed. This implies that the MSC active power provided by the rotor circuit is equal to the GSC active power $P_G = P_R$. Considering the GSC current as a function of the rotor power and reactive power reference value, the current source of the Norton equivalent circuit of the GSC can be determined:

$$\begin{aligned} \underline{i}_{qGSC} &= \underline{i}_{GSC} - \frac{\underline{u}_G}{\underline{Z}_{GSC}} \\ &= \frac{2}{3}\left(\frac{P_R + jQ_{G,ref}}{\underline{u}_G}\right)^* - \frac{\underline{u}_G}{\underline{Z}_{GSC}} \end{aligned} \tag{15}$$

The model structure of the simplified DFIG-based WT is depicted in Fig. 8. The interface variables to the aerodynamic model as well as to the pitch and speed controller are written in orange.

3.2 FSC-based WT model

Since the PI controllers of the MSC controller in Fig. 6 are assumed to be quasi-stationary, the d-component of the stator current reference value $i_{Sd,ref}$ can be calculated using the feed forward term of the outer power controller loop retransformed from the transient-voltage-oriented reference frame into the original reference frame of the SCIG. Since the SCIG is operated in the constant flux region, the q-component of the stator current is controlled at a constant value, which is known from the initialization procedure [8]. Taking into account both the d- and q-components, the stator current reference value can be determined in complex notation as follows:

$$\underline{i}_{S,ref} = \frac{2P_{ag,ref}}{3u'_{Sd}} + \left(j - \frac{u'_{Sq}}{u'_{Sd}}\right) i_{Sq} \tag{16}$$

Considering the quasi-stationary assumption of the inner current controller, the stator current is set to the stator current reference value, i.e., $\underline{i}_S = \underline{i}_{S,ref}$. The slip frequency $s_G\omega_S$ can be calculated from (6) under consideration of $\underline{u}_R = 0$ and $\dot{\underline{\psi}}_R = 0$:

$$s_G\omega_S = j\frac{R_R \underline{i}_R}{\underline{\psi}_R} \tag{17}$$

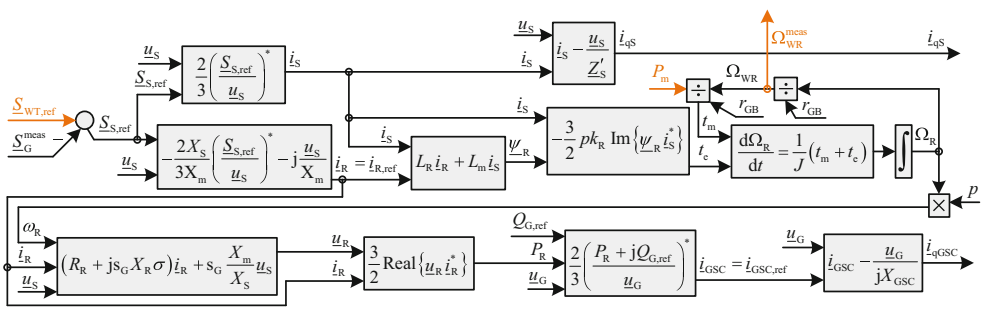

Fig. 8 Model structure of the simplified DFIG-based WT

Substituting $\underline{\psi}_R$ in (8) using $\underline{\psi}_R = \underline{u}'_S/\mathrm{j}\omega_S k_R$ and then rearranging the resulting equation leads to:

$$\underline{i}_R = \frac{\underline{u}'_S}{\mathrm{j}\omega_S k_R L_R} - \frac{L_m}{L_R}\underline{i}_S \tag{18}$$

Substituting (18) and $\underline{\psi}_R = \underline{u}'_S/\mathrm{j}\omega_S k_R$ in (17) and adding it to the rotor angular frequency ω_R leads to the equation of the stator angular frequency ω_S:

$$\omega_S = s_G\omega_S + \omega_R = \frac{\mathrm{j}\underline{u}'_S R_R + \underline{u}'_S L_R \omega_R}{\underline{u}'_S L_R - R_R k_R L_m \underline{i}_S} \tag{19}$$

The stator voltage can be obtained from the feed forward terms of the inner current controller loop re-transformed from the transient-voltage-oriented reference frame into the original reference frame of the induction generator in complex notation:

$$\underline{u}_S = \mathrm{j}\omega_S\left(L_S\underline{i}_S - k_R L_m i_{Sd}\right) \tag{20}$$

The rotor current as a function of the rotor flux linkage and the slip frequency can be obtained by rearranging (17). After substituting the resulted equation in (8) the equation of the rotor flux linkage, which is needed to calculate the electrical torque, can be obtained:

$$\underline{\psi}_R = \frac{L_m R_R \underline{i}_S}{R_R + \mathrm{j}L_R s_G \omega_S} \tag{21}$$

The same underlying assumptions made regarding the GSC of the DFIG-based WT, are equally valid for the FSC based WT. Considering the GSC current as a function of the stator power and reactive power reference value, the current source of the Norton equivalent circuit of the GSC can be determined:

$$\begin{aligned}\underline{i}_{qGSC} &= \underline{i}_{GSC} - \frac{\underline{u}_G}{\underline{Z}_{GSC}} \\ &= \frac{2}{3}\left(\frac{P_S + \mathrm{j}Q_{G,ref}}{\underline{u}_G}\right)^* - \frac{\underline{u}_G}{\underline{Z}_{GSC}}\end{aligned} \tag{22}$$

The model structure of the simplified FSC-based WT is depicted in Fig. 9. The interface variables to the aerodynamic model as well as to the pitch and speed controller are written in orange.

3.3 Norton equivalent circuits

Equation (23) demonstrates the positive sequence of the overall network nodal equation system, where the fundamental oscillations of voltages and currents are considered through their RMS values [8]:

$$\underline{\mathbf{Y}}_N\underline{\mathbf{u}} = \underline{\mathbf{Y}}\mathbf{u} + \underline{\mathbf{i}}_q \tag{23}$$

The WT models as well as other active devices (e.g. generating units and their respective control systems, dynamic loads, etc.) are considered by their Norton equivalent circuits, whose admittance equations in the matrix notation are represented on the right side of (23), where $\underline{\mathbf{Y}}$ is a diagonal matrix whose diagonal elements are occupied by the internal admittances of the active devices. The quantities $\underline{\mathbf{u}}$ and $\underline{\mathbf{i}}_q$ represent the nodal voltage and the current source vectors. The passive electrical network connects the active device models and is considered by its steady-state model, whose admittance equation in matrix notation is-

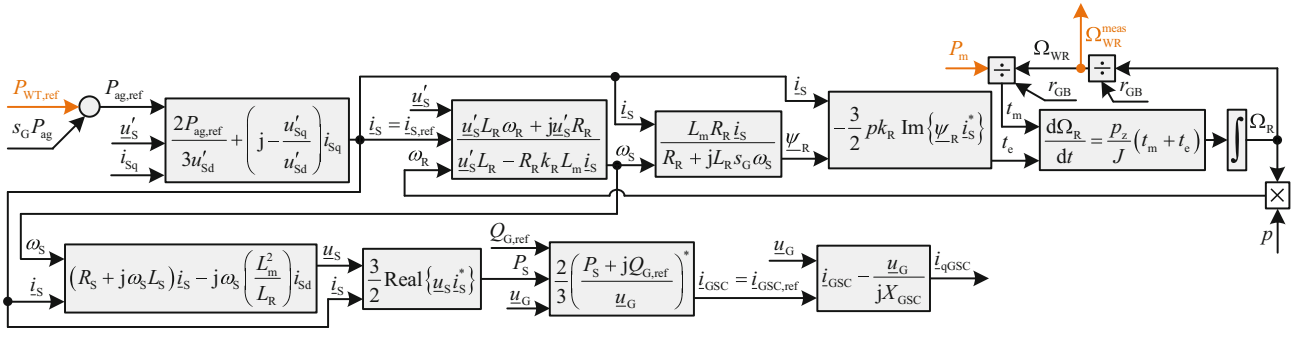

Fig. 9 Model structure of the simplified FSC-based WT considering stator resistance

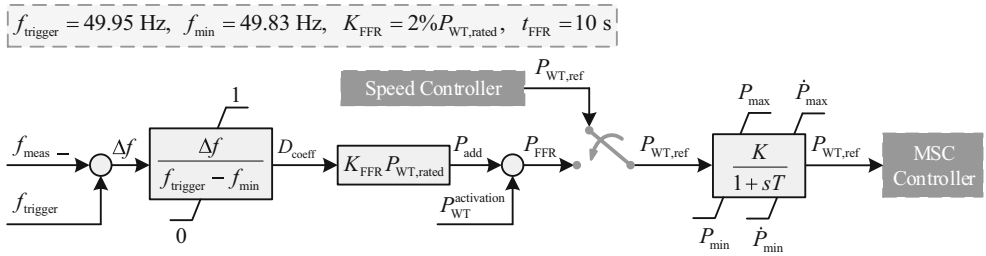

Fig. 10 Control structure of the implemented FFR controller [8]

represented on the left side of (23), where $\underline{\mathbf{Y}}_N$ indicates the network admittance matrix including the static loads. The network nodal voltages at each time step are calculated by rearranging (23), as demonstrated in (24).

$$\underline{\mathbf{u}} = \left(\underline{\mathbf{Y}}_N - \underline{\mathbf{Y}}\right)^{-1} \underline{\mathbf{i}}_q \tag{24}$$

While the current sources of the detailed WT models depend on the state variables of the differential equations at each time step, the current sources of the simplified WT models at each time step are calculated using the terminal voltages of the last time step (see 14, 15, 22), which are obtained from (24). The resulting current sources are used to obtain the terminal voltages at the current time step, which serve as input variables of the WT model structures, as illustrated in Figs. 8 and 9. This algebraic dependency between the current sources and the terminal voltages should be considered utilizing appropriate methods. Two possible approaches are taken into account in this paper. The first approach is to reduce the time step size to such an extent that the voltage difference between two time steps is imperceptibly small, so that they have no influence on the results. Adoption of this solution leads to a higher computational time, which is not purposeful when simulating large grid areas in the time frame of interest of the frequency stability analysis. In the second approach, the algebraic loops are solved iteratively at each time step. Considering this solution, the time step size can even be increased considerably, which will lead to a significant reduction in computational time. The results of both methods are illustrated and compared to each other in Sect. 6.

4 Fast frequency response controller

FFR is a measure to improve the frequency behavior of a power system with a high-level penetration of PEGU during disturbance events. It is defined in [5] as a reaction of power park modules in the very first seconds of a frequency drop by quickly activating the active power contribution to counteract the effects of low system inertia. The FFR controller implemented in this paper is a droop-based one, which reacts to a grid frequency below a predefined trigger threshold by temporarily increasing the active power and is introduced in [2] referred to as ENERCON IE (see Fig. 10). The additional energy to cover this power is extracted from the rotating mass of the WT as a result of its deceleration. The rate of change of frequency (ROCOF) and the frequency nadir (FN) are two key indicators in evaluating frequency stability studies, which is why they are given special consideration in this context. Since this control system does not provide a response proportional to ROCOF and thus cannot deliver an inherent frequency response like a synchronous generator, often termed "true inertial response", it cannot affect the ROCOF, but only contributes to improving the FN.

As shown in Fig. 10, the active power set point of the MSC controller is provided by the FFR controller and the speed controller becomes deactivated when the measured frequency drops below the trigger frequency. In FFR mode, the deviation of f_{meas} from $f_{trigger}$ enters the controller, while the sum of the WT active power output at the time of FFR activation $P_{WT}^{activation}$ and an additional power signal P_{add} is provided as the output variable. The additional power signal exhibits the following linear dependency on the frequency deviation:

$$P_{add} = \underbrace{\frac{f_{trigger} - f_{meas}}{f_{trigger} - f_{min}}}_{D_{coeff}=0<\cdots<1} K_{FFR} P_{WT,rated} \tag{25}$$

The term $K_{FFR} P_{WT,rated}$ as the maximum possible additional power is set to a proportion of the WT rated active power and is fully provided when the measured frequency reaches the frequency limit f_{min}. As can be dervived from (25), the range of the droop coefficient D_{coeff} varies between 0 and 1. For better illustration, Fig. 11 represents the droop characteristic of the FFR controller, which shows the relationship between D_{coeff} and f_{meas}. Once the measured frequency exceeds the trigger frequency or the activation time t_{FFR} has elapsed, the FFR mode is deactivated. Consequently, the speed controller provides the active power set point of the MSC controller again. The PT1 element of the speed controller enables a smooth re-acceleration of the WT to the operating point prior to the FFR activation. Having a smooth recovery period prevents the power system from perceiving the re-acceleration of the WTs as a second severe frequency drop. The controller parameters chosen in this paper are shown on top of the Fig. 10.

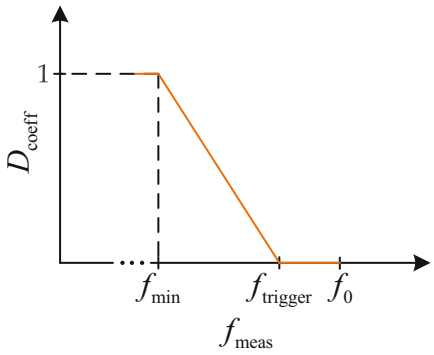

Fig. 11 Droop characteristic of the FFR controller

5 Advantages of the simplified WT models

As mentioned in Sect. 1, the advantages of the simplified WT models over the detailed RMS WT models are the significant reduction in the number of state variables of the models as well as the increase in the size of the simulation time step. Table 1 gives an overview of the state variables of the simplified and the detailed WT models. As shown in Table 1, while the number of state variables for the detailed DFIG- and FSC-based WTs is 20 respectively 19, the number for each of the two simplified models is 6, which leads to a significantly lower model complexity and thus to a considerably lower parametrization effort. The typical simulation time step size of RMS simulations including only conventional active devices (i.e., synchronous generators and dynamic loads) is about 10 ms. Consideration of the detailed RMS WT models in the simulation results in smaller simulation time steps down to 1 ms due to comparatively smaller time constants of the converter controllers [10]. Applying the simplified WT models instead of the detailed ones in the RMS simulations performed in the case studies presented in the next section offers the advantage of increasing the simulation time step size up to 12 ms without loss of accuracy. This leads to a significantly lower computational time and effort in large-scale studies considering a high share of WTs.

Table 1 State variables of simplified (s.) and detailed (d.) WT models

	DFIG		FSC	
	d.	s.	d.	s.
Wind turbine rotor speed	✓	X	✓	X
Generator rotor speed	✓	✓	✓	✓
Mechanical angle difference	✓	X	✓	X
Low-pass filter of aerodynamic model	✓	✓	✓	✓
Speed controller	✓	✓	✓	✓
Power ramp limiter	✓	✓	✓	✓
Pitch controller	✓	✓	✓	✓
Pitch actuator	✓	✓	✓	✓
d-comp. of power controller of MSC	✓	X	✓	X
q-comp. of power controller of MSC	✓	X	X	X
d-comp. of current controller of MSC	✓	X	✓	X
q-comp. of current controller of MSC	✓	X	✓	X
d-comp. of the rotor flux linkage	✓	X	✓	X
q-comp. of the rotor flux linkage	✓	X	✓	X
DC voltage	✓	X	✓	X
DC voltage controller	✓	X	✓	X
d-comp. of current controller of GSC	✓	X	✓	X
q-comp. of current controller of GSC	✓	X	✓	X
PLL of MSC	✓	X	✓	X
PLL of GSC	✓	X	✓	X

6 Case studies

The simulation results presented below serve as comparisons of the functionality and performance of the simplified WT models against those of the detailed WT models in the time frame of interest for frequency stability analysis.

6.1 Step response simulations

The first examples consist of step-response simulations of a 2 MW DFIG-based and a 2 MW FSC-based WT model each as a detailed and a simplified model and coupled to a 20 kV passive equivalent grid via a transformer (0.69/20 kV). The model parameters of both WT models used in this paper are identical and can be found in [7]. The initialization procedure of each WT model is performed based on the terminal output apparent power, which are known from a Newton-Raphson-based power flow calculation [15]. The initialization approaches used in this paper are extensively discussed in [8].

Some characteristic variables of step response simulations of both detailed WT models to different deterministic wind speeds are compared to those of both simplified WT models in Figs. 12 and 13. In each case, the wind speed is increased from 10 m/s to 14 m/s, with 1 m/s steps every 50 s, as shown in Figs. 12a and 13a. After 250 s, the operating points return to the initial values with the same step sizes. At wind speeds lower than 12 m/s, the speed controller controls the rotor speed according to the tracking characteristic curve (see Figs. 12c and 13c). The MSC controller of the detailed WT models controls the WT terminal active power to its reference value provided by the speed controller.

As mentioned in Sect. 3, taking into account the quasi-stationary assumption of the converter controllers of the simplified WT models, the reference values of the WT terminal active power are directly and without any delay considered in the calculation of the current sources of the Norton equivalent circuit of the MSC and GSC (see 14, 15 and 22). At wind speeds equal to or higher than 12 m/s, the pitch controller adjusts the rotor blade angle (Figs. 12a and 13a) by controlling the rotor speed and limits the mechanical

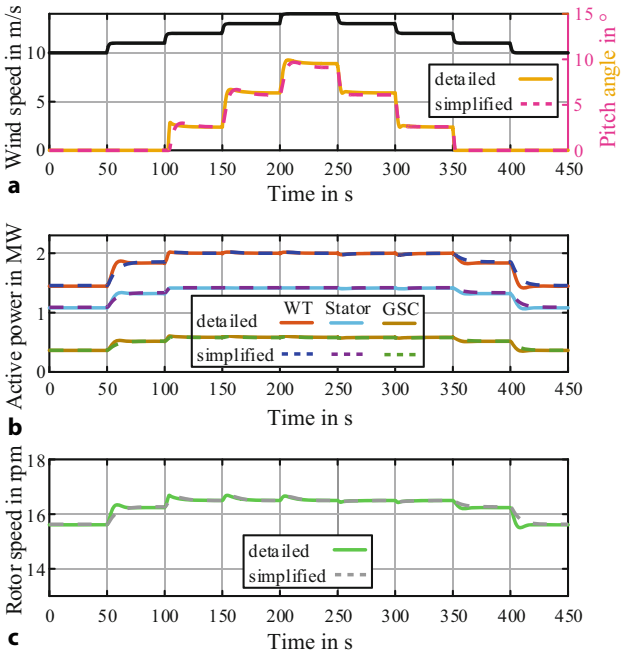

Fig. 12 Wind speed step responses of DFIG-based WT

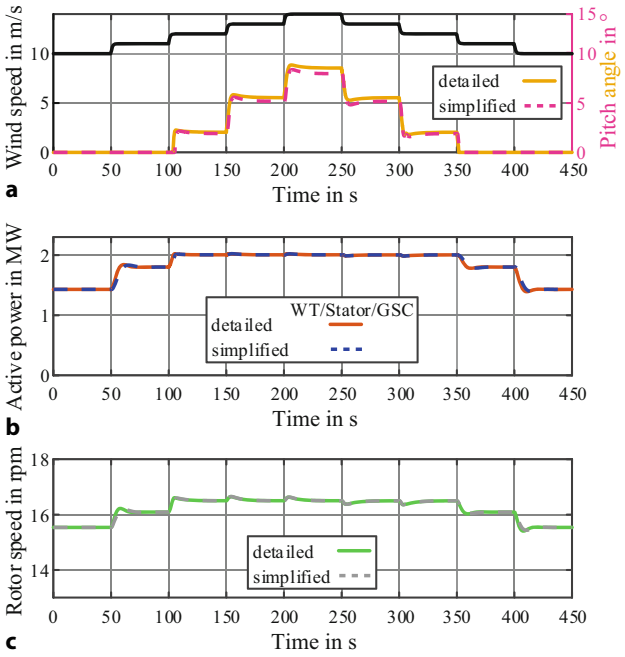

Fig. 13 Wind speed step responses of FSC-based WT

torque and consequently the output active power to the WT rated power (Figs. 12b and 13b). The output active power of the FSC-based WT is equal to the stator active power neglecting the converter losses. Its output reactive power is kept constant at the reference value of the GSC that is equal to the initial value of the WT terminal reactive power. The output active and reactive power of the DFIG-based WT are composed of the stator portion and the rotor circuit portion. The reactive power of the rotor circuit is kept at zero and the reactive power of the stator is kept constant at the initial value of the WT terminal reactive power over the whole simulation time. As shown in Figs. 12 and 13, the conducted comparison of the step response simulation results demonstrates an acceptable level of model accuracy of the simplified WT models against the detailed RMS WT models.

6.2 *Frequency response simulations*

In order to demonstrate the comparability of the contributions of the simplified WT models against the detailed WT models in improving the frequency performance of power systems, the WT models are extended with the droop-based FFR controller introduced in Sect. 4. Furthermore, the simplified as well as the detailed WT models are programmed in the MATLAB environment and are implemented in a MATLAB-based RMS simulation tool, which is discussed in [16, 17] and is referred to as a "distributed-rotating-mass based model".

The simulation tool does not utilize an infinite busbar and is therefore well suited for performing frequency studies. In this simulation tool, the synchronous generators are represented through a fifth-order state space model commonly called model 2.1, according to the IEEE Std 1110-2019 [11]. The excitation systems are modelled using a ST1C excitation system with a PSS1A stabilizer from the IEEE Std

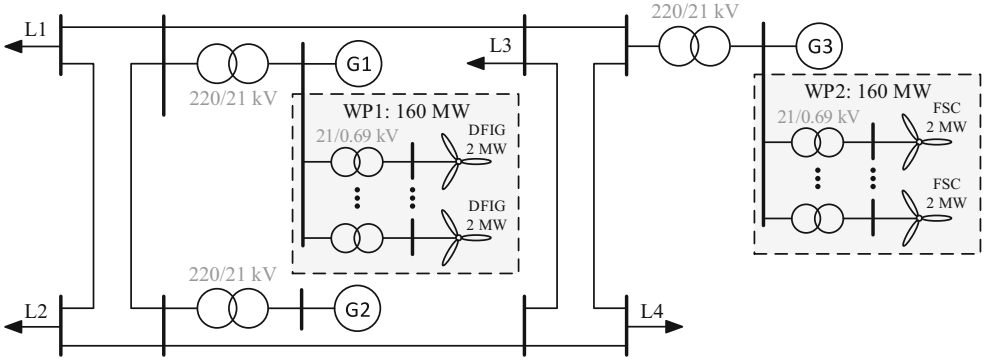

Fig. 14 The single line diagram of the 220 kV test system

Table 2 Steady-state terminal powers of the active devices in passive sign convention

	G1	G2	G3	WP1	WP2	L1	L2	L3	L4
Active power in MW	−347	−400	−400	−80	−80	300	350	350	300
Reactive power in Mvar	−87	−77	−80	−16	−16	20	25	30	20

421.5-2016 [12]. The prime mover models and their control systems, which are also discussed in [16], enable the simulation of primary and secondary control power activation in accordance with the specific regulatory requirements [3, 4]. The implemented composite load model comprises of a dynamic and a static component. The dynamic component is represented by a third-order induction motor and the static component by a ZIP model [1]. The passive network components (i.e., transformers and transmission lines) are represented by their steady-state models. The model parameters of all devices and their corresponding controllers used in this paper can be found in [17]. Fig. 14 shows the single line diagram of a 220 kV test system.

Four loads (L) are supplied by three synchronous generators (G) and two wind parks (WP) through a transmission grid. WP1 comprises 80 DFIG-based WTs and WP2 consists of 80 FSC-based WTs each with a rated active power of 2 MW. No aggregation of the WT models is performed in this paper. To determine the nodal voltages and powers at the considered operating point, a Newton–Raphson-based power flow calculation is conducted. The initial terminal apparent powers of the active devices (i.e., synchronous generators, loads and wind power plants) resulting from the power flow calculation are shown in Table 2.

Four scenarios with constant wind speed are simulated based on an unscheduled increase in load L1 by 45 MW after 10 s. In the scenario 1 the FFR controllers of all WTs are deactivated. Thus, only the synchronous generators offer their inertia to control the ROCOF and the FN. In the three remaining scenarios, fifty percent of the WTs in each WP provide FFR capabilities. These three scenarios differ with respect to the modeling depth, i.e., detailed (scenario 2) or simplified (scenario 3 and 4). In order to solve the algebraic loop resulting in the case of utilizing the simplified WT models, in scenario 3, the time step size reduction is applied, while the iterative approach is used in the scenario 4.

Figs. 15a and 16a show the power and rotor speed response of an exemplary DFIG-based WT from WP1 and an exemplary FSC-based WT from WP2, respectively, to the above-mentioned disturbance in the scenarios 2, 3 and 4 by means of the power–speed characteristic curves. Point A in each figure represents the stationary operating point before the perturbation in each scenario. If the grid frequency exceeds the threshold, the FFR controller is triggered and thus

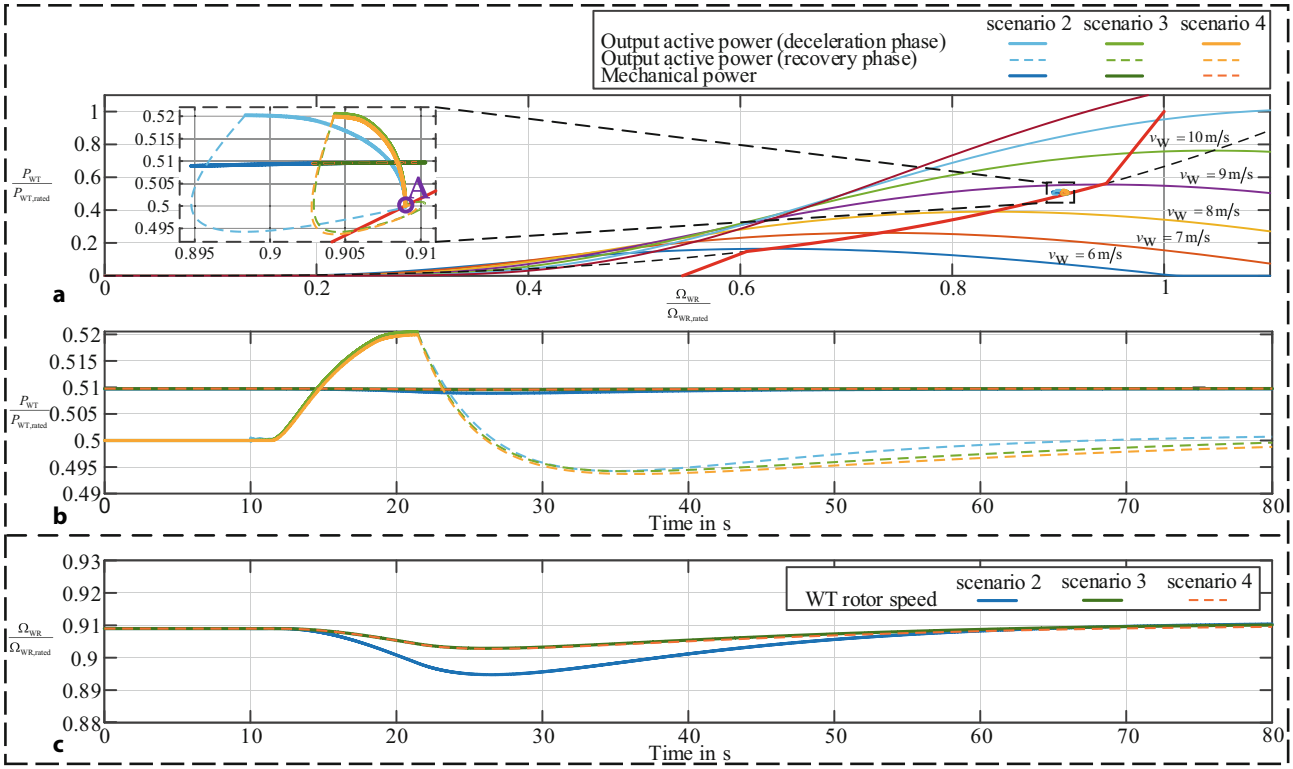

Fig. 15 Power and speed responses of an exemplary DFIG-based WT in scenarios 2, 3 and 4

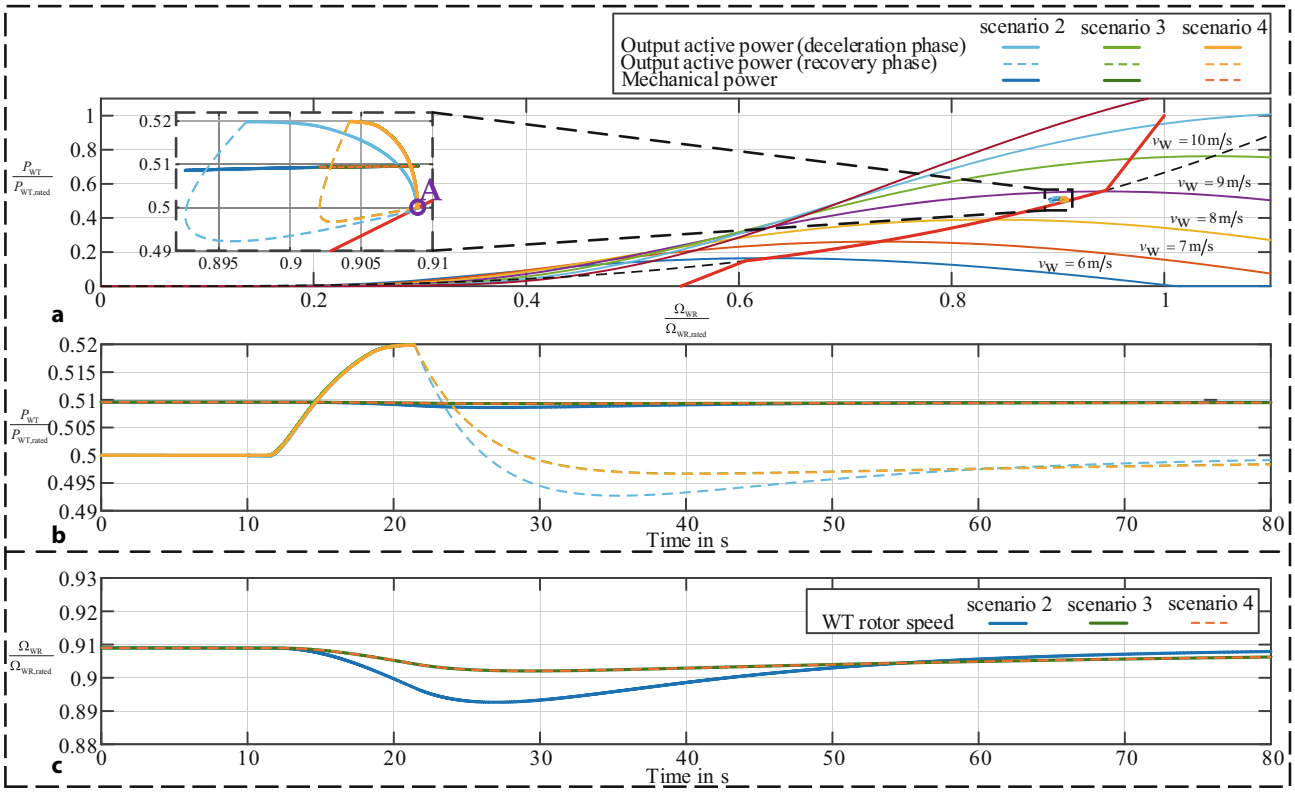

Fig. 16 Power and speed responses of an exemplary FSC-based WT in scenarios 2, 3 and 4

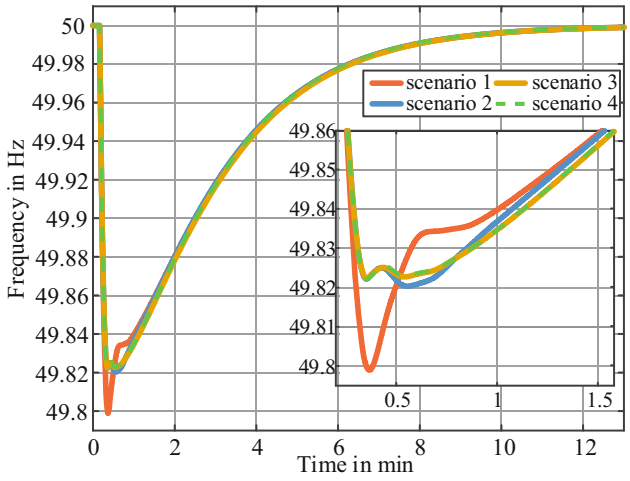

Fig. 17 Center of inertia frequency in scenarios 1, 2, 3, 4

the sum of $P_{WT}^{activation}$ and P_{add} is commanded to the MSC controller as the active power set point. In the overproduction phase (i.e., the solid curves), since the electrical output power plus the WT losses are higher than the available mechanical power extracted from the wind, the rotating mass of the WT decelerates, and the rotor speed decreases. The slope of the solid curves can be modified by setting the minimum frequency limit f_{min}. The higher this frequency is set, the steeper the solid curves become. Once the activation time period t_{FFR} is over, the speed controller is activated and the recovery phase (i.e., the dashed curves) begins with the goal of accelerating the WT back to the desired operating point on the tracking characteristic curve, which depends on the current wind speed. As the wind speed is constant in all scenarios, the desired rotor speed is the same as the pre-fault rotor speed (i.e., point A). Fig. 15b and c as well as Fig. 16b and c demonstrate the mechanical power, the output active power and the WT rotor speed of both selected WTs in the overproduction phase and the recovery phase in the time domain.

As shown in the time domain illustrations, the output active power curves in the overproduction phase and their peak values of both WT models in all three scenarios are identical. Furthermore, the output active power curves of the DFIG-based WT models in the recovery phase are very good comparable in all three scenarios. On the other hand, the output active power curve of the FSC-based WT model falls slightly lower in the recovery phase in scenario 2 and continues with a higher slope compared to scenarios 3 and 4. As illustrated in Fig. 15a and c as well as in Fig. 16a and c, the rotor speed of both selected WTs exhibits a more dynamic behavior in scenario 2 and falls insignificantly lower compared to scenarios 3 and 4. As it is observed, this dynamic behavior has no effect on the output variable of the FFR controller of both WT models, which directly sets the reference value of output active power to the MSC controller.

Fig. 17 depicts the center of inertia frequencies in all four scenarios mentioned above. As shown in the figure, very good comparable frequency responses with respect to the FN are observed in scenarios 2, 3 and 4, i.e. similar improvements of the FN are observed in all three scenarios. However, the frequency responses differ slightly regarding the undesirable but unavoidable second frequency drop caused by the power reduction in the recovery phase, which is deeper the higher the maximum additional power achieved in the overproduction phase. This observed difference is due to the fact that the output active power curve of the FSC-based WT model falls slightly lower in the recovery phase in scenario 2 compared to scenarios 3 and 4, as depicted in Fig. 16. This deviation is not relevant for the evaluation of the test system's frequency response, because it has no influence on the two important frequency stability indicators, i.e., ROCOF and FN.

7 Conclusion

This article presents efficient simulation models of a DFIG-based WT and a FSC-based WT based on induction generator, which are derived from detailed RMS WT models based on fundamental machine and converter equations. The modeling efficiency primarily refers to the negligence of state variables of the WT models corresponding to very small time constants without significant effects on their behavior within the time frame of interest of frequency stability analysis. These model simplifications lead to considerable reductions in the number of state variables of the simplified WT models and thus to lower model complexities as well as lower parametrization effort compared to the detailed RMS WT models, which are traditionally used for analyzing the frequency stability of power systems.

While the number of state variables for the detailed DFIG- and FSC-based WTs is 20 respectively 19, the number for each of the two simplified models is 6. Furthermore, the underlying simplifications enable higher simulation time steps from 1 ms up to 12 ms, which lead to a significant reduction in computational time in large-scale studies with a high WT penetration.

In order to verify the validity of the underlying simplifications, the simplified WT models are compared against the detailed RMS WT models with particular emphasis on their general behavior in case of step responses to different deterministic wind speeds and their frequency responses in the event of a frequency drop in a 220 kV test system. The step response simulations are performed by connecting a 2 MW DFIG-based and a 2 MW FSC-based WT model each as a detailed and simplified model to a 20 kV passive equivalent grid via a transformer (0.69/20 kV). A comparison of the simulation results demonstrates an acceptable level of model accuracy of the simplified WT models against the detailed ones. In order to demonstrate the comparability of contributions of the simplified WT models and the detailed ones in improving the frequency performance of power systems, both the detailed RMS WT models as well as the simplified WT models are extended with a droop-based FFR controller. The simulation results show plausible and very good comparable frequency responses with respect to the FN.

Funding Open Access funding enabled and organized by Projekt DEAL.

References

1. CIGRÉ C4605 (2014) Technical brochure 566: Modelling and aggregation of loads in flexible power networks
2. Engelken S, Mendonca A, Fischer M (2017) Inertial response with improved variable recovery behaviour provided by type 4 WTs. IET Renew Power Gener 11(3):195–201. https://doi.org/10.1049/iet-rpg.2016.0333
3. ENTSO-E (2004) Appendix 1: Load-frequency control and performance. https://eepublicdownloads.entsoe.eu/clean-documents/pre2015/publications/entsoe/Operation_Handbook/Policy_1_Appendix%20_final.pdf. Accessed 09.10.2022
4. ENTSO-E (2009) Policy 1: Load-frequency control and performance. https://eepublicdownloads.entsoe.eu/clean-documents/pre2015/publications/entsoe/Operation_Handbook/Policy_1_final.pdf. Accessed 09.10.2022
5. ENTSO-E (2018) Need for synthetic inertia (SI) for frequency regulation. https://eepublicdownloads.entsoe.eu/clean-documents/Network%20codes%20documents/NC%20RfG/IGD_Need_for_Synthetic_Inertia_final.pdf. Accessed 09.10.2022
6. Erlich I, Wilch M (2010) Primary frequency control by wind turbines. In: IEEE PES General Meeting, IEEE, Minneapolis, MN, pp 1–8 https://doi.org/10.1109/PES.2010.5589911
7. Feltes C (2012) Advanced fault ride-through control of DFIG based wind turbines including grid connection via VSC-HVDC. Berichte aus der Energietechnik. Shaker, Aachen
8. Goudarzi F, Hofmann L (2021) A combined RMS simulation model for DFIG-based and FSC-based wind turbines and its initialization. Energies 14(23):8048. https://doi.org/10.3390/en14238048
9. Heier S (2014) Grid integration of wind energy, 3rd edn. John Wiley & Sons Inc, Chichester
10. Hennig T, Hofmann L, Erlich I (2018) Auswirkungen eines vermaschten Offshore-Netzes in HGÜ-Technik auf die Netzführung der angeschlossenen Verbundsysteme. Berichte aus der Elektrotechnik. Shaker, Aachen

11. IEEE Std 1110-2019 (2020) Ieee std 1110-2019 – IEEE guide for synchronous generator modeling practices and parameter verification with applications in power system stability analyses https://doi.org/10.1109/IEEESTD.2020.9020274
12. IEEE Std 421.5-2016 (2016) IEEE std 421.5-2016 – IEEE recommended practice for excitation system models for power system stability studies https://doi.org/10.1109/IEEESTD.2016.7553421
13. Kundur P, Balu NJ, Lauby MG (1994) Power system stability and control. McGraw-Hill, New York
14. Mende D, Hennig T, Akbulut A, Becker H, Hofmann L (2016) Dynamic frequency support with DFIG wind turbines — a system study. In: 2016 IEEE Electrical Power and Energy Conference (EPEC), IEEE, Ottawa, ON, Canada, pp 1–7 https://doi.org/10.1109/EPEC.2016.7771694
15. Oswald BR (2021) Berechnung von Drehstromnetzen: Berechnung stationärer und nichtstationärer Vorgänge mit Symmetrischen Komponenten und Raumzeigern, 4th edn. Springer Vieweg, Wiesbaden
16. Pawellek A, Hofmann L (2018) Comparison of methods for the simulation of dynamic power flows in the international grid control cooperation. In: 2018 IEEE Electronic Power Grid (eGrid), IEEE, Charleston, SC, pp 1–6 https://doi.org/10.1109/eGRID.2018.8598698
17. Pawellek A, Hofmann L, Wolter M (2021) Entwicklung und Modellierung von Konzepten für das Engpassmanagement im Netzregelverbund. Berichte aus dem IfES. TEWISS, Garbsen
18. Rakhshani E, Gusain D, Sewdien V, Rueda Torres JL, Van Der Meijden MAMM (2019) A key performance indicator to assess the frequency stability of wind generation dominated power system. IEEE Access 7:130957–130969. https://doi.org/10.1109/ACCESS.2019.2940648
19. Rakhshani E, Rueda Torres JL, Palensky P, van der Meijden M (2019b) Determination of maximum wind power penetration considering wind turbine fast frequency response. In: 2019 IEEE Milan PowerTech, IEEE, Milan, Italy, pp 1–6 https://doi.org/10.1109/PTC.2019.8810492
20. Sewdien VN, van der Meijden M, Breithaupt T, Hofmann L, Herwig D, Mertens A, Tuinema BW, Rueda Torres JL (2018) Effects of increasing power electronics on system stability: Results from MIGRATE questionnaire. In: 2018 International Conference and Utility Exhibition on Green Energy for Sustainable Development (ICUE), IEEE, Phuket, Thailand, pp 1–9 https://doi.org/10.23919/ICUE-GESD.2018.8635602

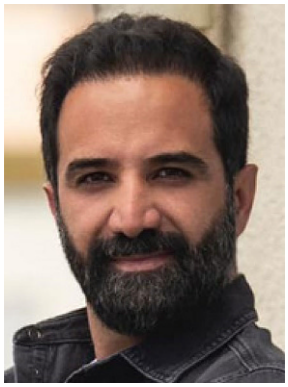

Farshid Goudarzi, received the M.Sc. degree in power engineering from Leibniz Universität Hannover, Hanover, in 2015, where he is currently pursuing the Ph.D. degree in electrical engineering from the Institute of Electric Power Systems. His research interests include dynamic simulation of extensive electrical energy systems and power system stability studies under consideration of high penetration of power electronic-interfaced generating units.

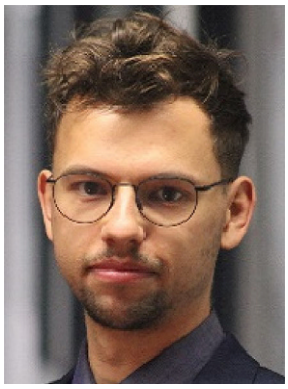

Lucas Reus, was born in Gehrden, Lower Saxony, Germany, in 1994. He received the M.Sc. degree in power engineering from Leibniz University Hannover, Hanover, in 2021, where he is currently pursuing the Ph.D. degree in electrical engineering from the Institute of Electric Power Systems. His research interests include dynamic simulation of power systems and operation of power systems with a high share of power electronic-interfaced generating units.

Lutz Hofmann, was born in Bad Oeynhausen, North Rhine-Westphalia, Germany, in 1968. He received the Dipl.-Ing. and Dr.-Ing. degrees from Leibniz Universität Hannover, Hanover, Germany, in 1994 and 1997, respectively. In 2002, he concluded his professorial dissertation in electric power engineering. In 2002 and 2003, he was a Project Manager at the engineering and consultant company Fichtner, Stuttgart, Germany. From 2004 to 2007, he was with the Network Planning Department, German transmission system operator E.ON Netz GmbH, Bayreuth, Germany. Since 2007, he has been a Full Professor and the Head of the Institute of Electric Power Systems, Leibniz Universität Hannover. Since 2011, he is also with the Fraunhofer IEE, Kassel, Germany. His current research interests include modeling and simulation of electric power systems, integration of renewable and decentralized energy sources, and power quality.